

# Recirculation of Purged Flow in an Adiabatic Counterflow Rotary Dehumidifier

J. J. Jurinak  
Assoc. Mem. ASME

J. W. Mitchell  
Mem. ASME

University of Wisconsin  
Solar Energy Laboratory,  
Madison, Wis. 53706

*The average process stream outlet humidity ratio of an adiabatic counterflow dehumidifier can be lowered if a portion of the process outlet stream is purged from the bulk flow. The purged stream can be recirculated and introduced at the inlet of the regenerating period. In this paper, the performance of such a purged counterflow dehumidifier is studied. Two purge geometries that result in a spatially nonuniform inlet condition in the regenerating period are considered. Wave diagram solutions for the limiting case of infinite heat and mass transfer coefficients are used to qualitatively predict the behavior of the purged dehumidifier. A finite difference solution is used to verify the general trends of the approximate wave diagram solutions. The effect of the recirculated purge on the process stream outlet states of high performance silica gel dehumidifiers with low and high thermal capacitance matrices operated at nearly optimal rotational speeds is evaluated.*

## Introduction

Counterflow rotary dehumidifiers are used in industrial air driers [1] and in energy-efficient, open-cycle desiccant air conditioners [2-5]. Considerable effort has been made to optimize the dehumidifier performance [4-8].

The performance of the adiabatic rotary dehumidifier can be improved by purging high-temperature, wet air from the dehumidified air stream, as shown schematically in Fig. 1. In steady-state operation, the air streams emerging from the dehumidifier have circumferential distributions of temperature and humidity ratio [9-11]. The air that exits in the first 10 to 20 percent of the rotational arc of the process period is considerably hotter and wetter than the rest of the dehumidified air stream. If this hot and wet air is physically removed from the process stream before mixing occurs, the mean temperature and humidity ratio of the process outlet air stream can be lowered. The purged air stream may be discarded, but since it is at high temperature, it can be recirculated and used in the regenerating period. The recirculated purge stream may either be mixed with the bulk regenerating stream or used to produce a locally nonuniform distribution in the regenerating period inlet. Recirculation of purged flow can both increase the dehumidification in the process stream and decrease the energy input to the regenerating stream. In addition, if the regenerating stream is heated by an open flame, the purge section can prevent contamination of the process air stream with combustion byproducts. The purged rotary dehumidifier has been used in prototype, open-cycle, desiccant air-conditioning systems developed by the Garrett Corporation and the Institute of Gas Technology [4, 5]. The effect of purging on open-cycle desiccant cooling system performance has been studied [13].

Adiabatic counterflow dehumidifiers with purged air recirculation and a spatially nonuniform regenerating stream inlet state are analyzed in this paper. Only balanced (equal  $v_{jk}$ ) and symmetric (equal  $\theta_j$ ) dehumidifiers are considered. The limiting case of a dehumidifier with infinite heat and mass transfer coefficients is studied first, using an approximate analogy with heat transfer regenerators. This analysis qualitatively shows the effect of purge recirculation on the dehumidifier performance. A finite difference model of the dehumidifier is then used to determine the outlet and purge states of a counterflow silica gel dehumidifier with

finite transfer coefficients. Typical silica gel properties are used, and the heat and mass transfer rates are assumed to be limited by convection. Both low and high thermal capacitance matrices are modeled, corresponding to matrices with small and large proportions of nonadsorbing structural materials. The numerical results are used to verify the trends suggested by the analogy analysis and to indicate the improvement in dehumidification and reduction in energy input obtained with recirculated purge in comparison to an unpurged counterflow dehumidifier.

## The Purged Dehumidifier Model

In the recirculation pattern illustrated in Fig. 1, flow from the outlet of subperiod 1 of period 1 is recirculated to the inlet of subperiod 1 of period 2 and is referred to as the preconditioning purge or recirculation pattern. A postconditioning purge geometry, with recirculation to subperiod 2 of the regenerating period, is also considered. The fractional subperiod boundaries are described by  $\beta_{jk} = \phi_{jk}/\Phi_j$ . For example,  $\beta_{11} = 0.10$  implies that the purge section occupies 10 percent of the total arc of period 1.

In this study, the following assumptions concerning the flow and transfer processes in the counterflow rotary dehumidifier are made: (i) the flow in each subperiod is at constant pressure and velocity; (ii) the flow at each subperiod inlet is at uniform temperature and humidity ratio; (iii) there is negligible axial diffusion of heat or moisture in the matrix and air; (iv) the thermal and moisture capacitances of the air in the matrix interstices are negligible compared to the matrix capacitances; (v) there is no transfer flux coupling by thermo-

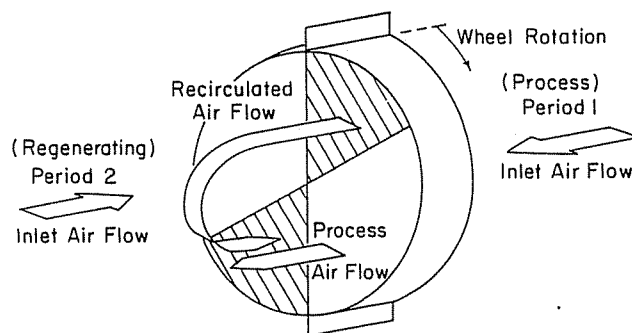


Fig. 1 Counterflow dehumidifier with preconditioning recirculation of purged flow

Contributed by the Heat Transfer Division for publication in the JOURNAL OF HEAT TRANSFER. Manuscript received by the Heat Transfer Division August 30, 1982.

diffusion or Dufor processes; ( $\nu i$ ) the transfer processes between the air and the matrix can be described by composite transfer coefficients.

The conservation equations written with respect to a coordinate system moving with the matrix are [9, 10]:

Mass

$$\frac{\partial w}{\partial x'} + \beta_{jk} \theta_j' (\mu\kappa)_{jk} \frac{\partial W}{\partial \theta'} = 0 \quad j, k = 1, 2 \quad (1)$$

Energy

$$\frac{\partial i}{\partial x'} + \beta_{jk} \theta_j' (\mu\kappa)_{jk} \frac{\partial I}{\partial \theta'} = 0$$

The transfer rate equations for mass and heat are

Mass

$$\frac{\partial w}{\partial x'} = \Lambda_{jk} (w_m - w_f) \quad j, k = 1, 2 \quad (2)$$

Energy

$$\frac{\partial i}{\partial x'} = \Lambda_{jk} (Le_o c_f (t_m - t_f) + i_{wv} (w_m - w_f))$$

Since the coordinate system is fixed with respect to the matrix, the rotary nature of the dehumidifier is modeled using periodic boundary conditions. The counterflow geometry is reflected by a reversal in flow direction at the beginning of each period. The recirculation condition is imposed by taking the spatial average of the outlet temperature and humidity ratio in the purge section to be the inlet condition for the appropriate subperiod in the regeneration period. The conservation of mass requires that  $\mu\kappa$ , the ratio of matrix rotational mass flow rate to air flow rate, in the two purge subperiods be equal (e.g.,  $\mu\kappa_{11} = \mu\kappa_{21}$  for the preconditioning purge).

### Equilibrium Analysis of the Purged Dehumidifier

If the transfer coefficients in equations (2) are infinite, then equations (1) describe equilibrium changes in the local air and matrix moisture and enthalpy. Analysis of the equilibrium system provides both an intuitive understanding of the dehumidifier operation and an upper bound to dehumidifier performance.

Banks and Maclaine-cross have shown that by proper definition of combined heat and mass transfer potentials,  $F_1$  and  $F_2$ , and combined capacitance ratios,  $\gamma_1$  and  $\gamma_2$ , equations (1) can be transformed to

$$\frac{\partial F_i}{\partial x'} + \theta_j' \beta_{jk} C_{i,jk} \frac{\partial F_i}{\partial \theta'} = 0 \quad \begin{matrix} i=1,2 \\ j=1,2 \end{matrix} \quad (3)$$

where  $C_{i,jk} = \mu\kappa_{jk} \gamma_i$  [9, 14-16]. The combined potentials,  $F_1$  and  $F_2$ , and the combined capacitance ratios,  $\gamma_1$  and  $\gamma_2$ , are functions of the equilibrium thermal and sorption properties of the moist air-adsorbent system. Equations (3) are first-order kinematic wave equations that are exactly similar to the wave equation that describes the equilibrium heat transfer in a rotary sensible regenerator [12, 14]. Wave diagrams drawn on an  $x' - \theta'$  coordinate system can be used to solve wave equations of this form [12, 14, 15]. The  $F_i$  wave fronts propagate with velocities  $V_{i,jk} = 1/(\theta_j' \beta_{jk} C_{i,jk})$ . Since for all desiccants,  $\gamma_1 < \gamma_2$ , an  $F_1$  change wave traverses the matrix more rapidly than an  $F_2$  wave. If the  $\gamma_i$  are constant,  $F_i$  changes propagate as sharp discontinuities through the matrix, represented by a straight line on the wave diagram. For most sorbents, the  $\gamma_i$  are not constant, so that the velocity of the  $F_i$  wave fronts vary with matrix state and the fronts can change shape. A broadening wave front is represented by a fan of lines on the wave diagram. Finite transfer coefficients tend to broaden or smear the wave fronts [9, 12, 14, 15].

Wave diagrams for  $F_1$  and  $F_2$  have previously been used to solve equations (3) for dehumidifiers with uniform [9, 14, 15] and spatially nonuniform [18, 19] air inlet states. The qualitative description of unpurged dehumidifier operation provided by this solution technique has been verified by comparison with the results of finite difference models [9, 13-15]. The equilibrium  $F_i$  wave diagram solutions for the purged dehumidifier are given here, and are later substantiated and refined by presentation of the results of a finite difference model.

It is assumed that the desiccant properties of the balanced and symmetric dehumidifier are constant. Therefore,  $\beta_{jk} C_{i,jk} = C_{i,j}$ , the wave velocities in each subperiod are equal,  $V_{i,jk} = V_{i,j} = V_i$ , and  $F_i$  lines on wave diagrams do not change slope at subperiod boundaries. For convenience in discussion, the subscripts on  $\beta_{11}$ , the fractional purge angle, will be dropped.

The hot and wet air in the initial portion of the dehumidified air stream is due to an  $F_1$  wave at the

### Nomenclature

$c_f$  = moist air thermal capacitance [energy/(dry mass-temperature)]  
 $c_m$  = matrix thermal capacitance [energy/(dry desiccant mass-temperature)]  
 $C_{i,j}$  =  $(\mu\kappa)_j \gamma_i$  analogous rotational capacity rate of period  $j$  [dimensionless].  
 $C_{i,jk}$  =  $(\mu\kappa)_{jk} \gamma_i$  subperiod  $k$  of period  $j$  analogous rotational capacity rate ratio for the  $F_i$  potential [dimensionless]  
 $F_i$  =  $i$ th combined heat and mass transfer potential [dimensions arbitrary]  
 $i$  = moist air enthalpy [energy/dry mass]  
 $i_{wv}$  = water vapor enthalpy [energy/mass]  
 $I$  = matrix enthalpy [energy/dry mass]  
 $J_{i,j}$  =  $4h/(\rho' d_h c_f)$ , where  $h$  is the heat transfer coefficient,  $\rho'$  is the dry fluid density,  $d_h$  is the hydraulic diameter. The lumped matrix-fluid transfer coefficient per unit mass of fluid [time<sup>-1</sup>]  
 $J_{w,j}$  =  $4h_w/(\rho' d_h)$ , where  $h_w$  is the mass transfer coefficient,  $\rho'$  is the dry fluid density, and  $d_h$  is the

hydraulic diameter. The lumped matrix-fluid mass transfer coefficient per unit mass of fluid [time<sup>-1</sup>]  
 $L$  = axial flow length through the matrix [length]  
 $Le_o$  =  $J_{i,j}/J_{w,j}$ , overall Lewis number [dimensionless]  
 $t_{j,k,l}$  = temperature at face  $l$  of subperiod  $k$  of period  $j$   
 $v_j$  = air velocity in period  $j$  [length/time]  
 $v_{jk}$  = air velocity in subperiod  $k$  of period  $j$  [length/time]  
 $V_{i,jk}$  =  $1/(\theta_j' \beta_{jk} C_{i,jk})$ , velocity of the  $F_i$  change wave in subperiod  $k$  of period  $j$  [dimensionless]  
 $w$  = moist air humidity ratio [dimensionless]  
 $w_{j,l}$  = spatial average humidity ratio at face  $l$  of period  $j$  [dimensionless]  
 $w_{j,k,l}$  = spatial average humidity ratio at face  $l$  of subperiod  $k$  of period  $j$  [dimensionless]  
 $W$  = matrix water content [dimensionless]  
 $x$  = axial displacement through matrix measured from period entrance [length]  
 $x'$  =  $x/L$ , dimensionless axial position [dimensionless]  
 $\beta$  =  $\phi_{11}/\Phi_1$ , fractional purge angle  
 $\beta_{jk}$  =  $\phi_{jk}/\Phi_j$ , fraction of period  $j$  occupied by subperiod  $k$  [dimensionless]

regenerating state ( $F_{1r}$ ) [9, 13–15]. Therefore, there are two solutions to consider for each purge geometry, corresponding to whether or not the  $F_{1r}$  wave passes through the matrix within the arc of the purge section. If  $\beta < C_{1,1}$  (i.e.,  $C_{1,1} < 1$ ), the  $F_{1r}$  wave is not completely purged; conversely, if  $\beta \geq C_{1,1}$  ( $C_{1,1} \geq 1$ ), the  $F_{1r}$  wave is entirely within the purge section. In each case, it is assumed that the purged air is fully mixed prior to introduction at the inlet of a subperiod in period 2. Thus, the distribution of the purged outlet state is destroyed, but the mean purge state creates a nonuniform inlet condition in the regenerating period. The  $F_1$  and  $F_2$  wave diagrams for these four cases are illustrated in Figs. 2–5. Figures 2 and 4 are for  $\beta \leq C_{1,1}$ , corresponding to an incomplete purge of the regeneration  $F_1$  state, while Figs. 3 and 5 illustrate  $\beta > C_{1,1}$  cases. In all of these diagrams,  $p$  is the process inlet state,  $pr$  is the purge state,  $r$  is the regenerating state, and  $o$  is the process outlet state.

Figure 2 shows the wave diagrams for the preconditioning recirculation pattern with  $\beta \leq C_{1,1}$ . The purge state is the regenerating inlet state. The mean period 1 outlet state and the  $\theta'$  distribution of period 1 outlet states are unaffected by the purge recirculation and are the same as for an unpurged dehumidifier. The preconditioning purge with  $\beta \leq C_{1,1}$  shifts the process outlet state toward the period 1 intersection point, corresponding to improved dehumidification.

The  $F_i$  wave diagrams for the preconditioning recirculation with  $\beta > C_{1,1}$  are shown in Fig. 3. The purge state is between the period 1 intersection point and the regenerating inlet state. The distribution and mean of the period 1 outlet states are identical to those for the preconditioning purge with  $\beta \leq C_{1,1}$ . The process outlet state is at the intersection point of the  $F_{1p}$  and  $F_{2r}$  lines, and maximum dehumidification is obtained.

The solution for the postconditioning recirculation pattern with  $\beta \leq C_{1,1}$  is shown in Fig. 4. For constant  $\gamma_i$ , the  $F_i$  purge states are recycled through the matrix and are completely arbitrary. In a system with variable  $\gamma_i$  or finite transfer coefficients, the wave fronts smear, and the purge state, rather than being arbitrary, tends to the regenerating state. In this case, the postconditioning recirculation with  $\beta \leq C_{1,1}$  results in the same distribution of period 1 outlet states as the preconditioning recirculation with  $\beta \leq C_{1,1}$ . Regardless of the purge state, the process outlet state is identical to that for the preconditioning purge with  $\beta \leq C_{1,1}$ .

The postconditioning purge with  $\beta > C_{1,1}$  is illustrated in Fig. 5. The  $F_{2pr}$  state is again completely arbitrary. However,  $F_{1pr} = F_{1p}$ , and the matrix is uniformly at  $F_{1p}$  during period

1. If the wave fronts broaden, then  $F_{2pr} = F_{2r}$ , and the period 1 outlet is uniformly at the intersection point of the  $F_{1p}$  and  $F_{2r}$  characteristics. The process outlet state is at the period 1 intersection point, as it is for the preconditioning purge with  $\beta > C_{1,1}$ .

The equilibrium analysis of the recirculated purge dehumidifier indicates that while the  $\theta'$  distribution of the period 1 outlet states is influenced by the recirculation geometry, the process outlet state ( $t_{12,2}, w_{12,2}$ ) depends only on the magnitude of the purge angle  $\beta$  in relation to  $C_{1,1}$ . As  $\beta$  increases, the fraction of the flow through period 1 of the dehumidifier that goes to the process decreases. At  $\beta = C_{1,1}$ , just as the regenerating state  $F_1$  is completely purged, the minimum outlet humidity ratio is obtained. For  $\beta > C_{1,1}$ , there is no change in process outlet state, but the useful process flow rate is decreased. This suggests that the optimum purge angle regardless of the recirculation pattern is  $\beta = C_{1,1}$ .

### Numerical Analysis of the Purged Dehumidifier

In a dehumidifier, the transfer coefficients are finite and the  $\gamma_i$  are not constant. Therefore, an equilibrium analysis is only of qualitative utility, and a numerical solution of equations (1, 2) is required to fully investigate the performance of the purged dehumidifier. The finite difference solution used in this study was derived from a method developed by Maclaine-cross [9] that was previously used by the authors [6, 13, 17]. The difference equations are second order. Solutions are obtained for three grid sizes, and the results are quadratically extrapolated to zero grid size. The extrapolated solution is fourth order [9]. For the results given here, the errors in the system moisture and energy balances are less than 0.01 percent of the changes in humidity ratio or enthalpy from period inlet to outlet.

A symmetric and balanced counterflow silica gel dehumidifier is studied. The overall Lewis number is assumed to be unity, a condition satisfied if convection controls the heat and mass transfer rates. Typical silica gel properties are employed to characterize the desiccant [13, 17]. Results are presented for two matrices. In one, there is negligible contribution by the structural materials to the matrix thermal capacity, and the bulk specific heat of silica gel applies ( $c_m = 921 \text{ J/kg}\cdot^\circ\text{C}$ ). A matrix that is 50 percent mylar or 44 percent aluminum by volume is also considered ( $c_m = 3350 \text{ J/kg}\cdot^\circ\text{C}$ ) [6]. Solutions are presented for high-performance dehumidifiers with  $\Lambda_{jk} = 20.0$ . The ratios of matrix rotational mass flow rate to air mass flow rate considered are

### Nomenclature (cont.)

- $\gamma_i$  = analogous capacitance ratio for the  $F_i$  potential [dimensionless]  
 $\eta_{wp} = (w_{1,1} - w_{12,2}) / (w_{1,1} - w_{1,int})$  normalized dehumidification per unit process period flow [dimensionless]  
 $\eta_{wp}^* = (1 - \beta_{11})\eta_{wp}$  normalized dehumidification per unit total period flow [dimensionless]  
 $\theta$  = time from the beginning of period 1  
 $\theta_j$  = duration of period  $j$  [time]  
 $\theta_{jk}$  = duration of subperiod  $k$  of period  $j$  [time]  
 $\theta'$  =  $\theta/T$  rotational time divided by time for a complete revolution [dimensionless]  
 $\theta'_j$  =  $\theta_j/T$  fractional rotational time of period  $j$  [dimensionless]  
 $\kappa_{jk} = L / (v_{jk}\theta_{jk})$ , carry-over ratio [dimensionless]  
 $\Lambda_{jk} = J_{w,jk}L / v_{jk}$ , dimensionless mass transfer length [dimensional]  
 $\mu_j$  = dry period  $j$  matrix mass divided by dry fluid mass contained in matrix in period  $j$  [dimensionless]  
 $\phi_{jk}$  = angle associated with subperiod  $k$  of period  $j$  [radians]

- $\Phi_j$  = angle associated with period  $j$  [radians]  
 $T$  = time required for a complete wheel revolution

### Subscripts

- $f$  = evaluated at fluid state  
 $i$  = combined potential index  
 $int$  = evaluated at intersection point of  $F_1$  characteristic through the period  $j$  inlet state and the  $F_2$  characteristic through the period  $3-j$  inlet state  
 $j$  = period index  
 $k$  = subperiod index  
 $l$  = face index 1 = inlet, 2 = outlet  
 $m$  = evaluated at, or in equilibrium with, the matrix state  
 $o$  = time or spatial average process outlet state  
 $p$  = evaluated at the process inlet state  
 $pr$  = evaluated at the time or spatially averaged purge state  
 $r$  = evaluated at the regenerating inlet state

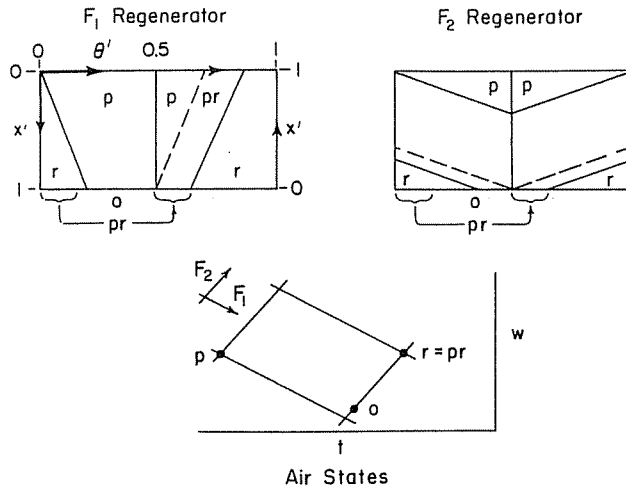


Fig. 2 Wave diagrams for the preconditioning purge with  $\beta \leq C_{1,1}$

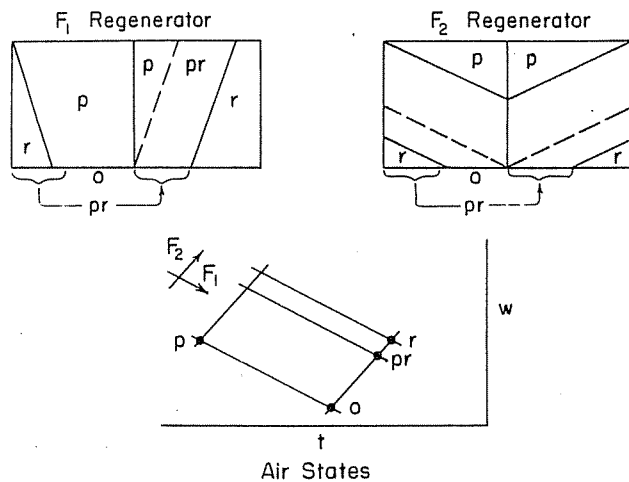


Fig. 3 Wave diagrams for the preconditioning purge with  $\beta > C_{1,1}$

Table 1 Inlet states, and the corresponding period 1  $F_i$  intersection points and outlet states for an unpurged dehumidifier with a low or high thermal capacitance matrix

	Inlet States ( $^{\circ}\text{C}, \text{g/kg}$ )		
	Process	Regenerating	
1	(35, 14.2)	(85, 14.2)	
2	(26.7, 11.1)	(85, 18.8)	
inlet state	matrix $c_m$	$(t_{1,int}, w_{1,int})$	$(t_{1,2}, w_{1,2})^a$
	( $\text{J/kg} \cdot ^{\circ}\text{C}$ )	( $^{\circ}\text{C}, \text{g/kg}$ )	( $^{\circ}\text{C}, \text{g/kg}$ )
1	921	(65.51, 3.846)	(66.0, 5.17)
	3350	(74.76, 3.959)	(70.2, 6.47)
2	921	(52.16, 2.151)	(55.6, 3.52)
	3350	(61.49, 1.219)	(62.6, 4.22)

$^a \Delta = 20.0$ ,  $Le_o = 1$ ,  $\mu_k = 0.20$  and  $0.125$  for low and high thermal capacitance matrices, respectively.

$\mu_k = 0.20$  for the bulk silica gel dehumidifier and  $\mu_k = 0.125$  for the high thermal capacity matrix. These  $\mu_k$  result in nearly maximum dehumidification of the process air stream in unpurged operation of the respective matrices [6, 17]. Two pairs of inlet states relevant to air conditioning processes are used. These are given in Table 1, along with the period 1  $F_i$  intersection points  $(t_{1,int}, w_{1,int})$  and the process outlet states  $(t_{1,2}, w_{1,2})$  for an unpurged dehumidifier with either the low or high thermal capacitance matrix.

The qualitative accuracy of the equilibrium analogy

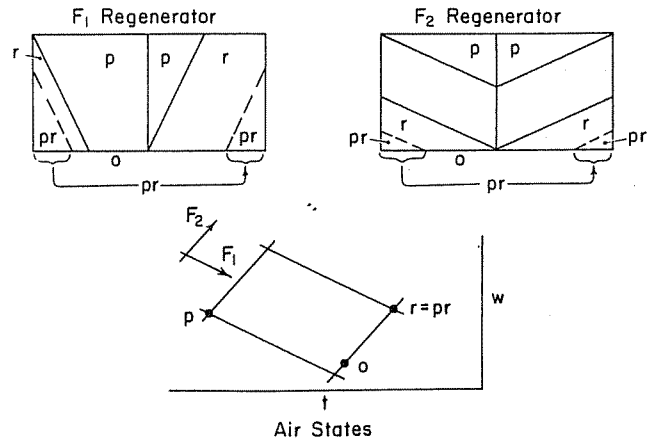


Fig. 4 Wave diagrams for the postconditioning purge with  $\beta \leq C_{1,1}$

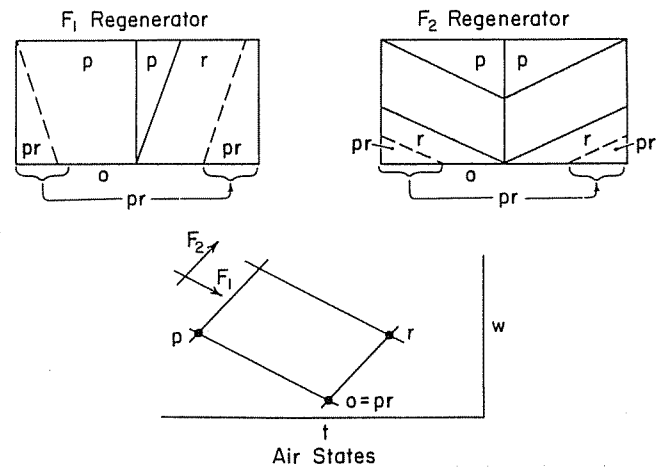


Fig. 5 Wave diagrams for the postconditioning purge with  $\beta > C_{1,1}$

Table 2 Finite difference solution for the purged dehumidifier with  $\beta < C_{1,1}$ ,  $\beta = C_{1,1}$ , and  $\beta > C_{1,1}$  for inlet state pair 1

	Period 1 mean		Purge		Process	
	$t(^{\circ}\text{C})$	$w(\text{g/kg})$	$t(^{\circ}\text{C})$	$w(\text{g/kg})$	$t(^{\circ}\text{C})$	$w(\text{g/kg})$
<i>Precond.</i>						
$\beta = 0.025$	65.96	5.167	84.96	14.164	65.46	4.937
0.0875	65.94	5.171	81.50	11.564	64.43	4.558
0.150	65.86	5.187	76.73	8.945	63.93	4.524
<i>Postcond.</i>						
$\beta = 0.025$	65.95	5.164	84.85	14.064	65.46	4.936
0.0875	65.11	4.689	72.98	6.438	64.35	4.521
0.150	64.34	4.478	66.71	4.271	63.92	4.515

solutions is demonstrated by the period 1 outlet air temperature and humidity ratio distributions shown in Figs. 6 and 7 for the preconditioning and postconditioning recirculation patterns. A low thermal capacitance dehumidifier with inlet state pair 1 and  $\mu_k = 0.20$  is considered. For this case,  $C_{1,1} = 0.0875$  [17], so that the selected range of  $\beta$  spans incomplete and complete purging of the  $F_{1,r}$  state. Table 2 gives the period 1 mean outlet state, the mean purge state, and the mean process outlet state for the cases considered.

The equilibrium solutions indicate that the purge angle  $\beta$  does not affect the period 1 outlet temperature and humidity ratio distributions in the preconditioning purge geometry. This is substantiated by the finite difference results given in Fig. 6 and Table 2. The variation with  $\beta$  of the spatial average

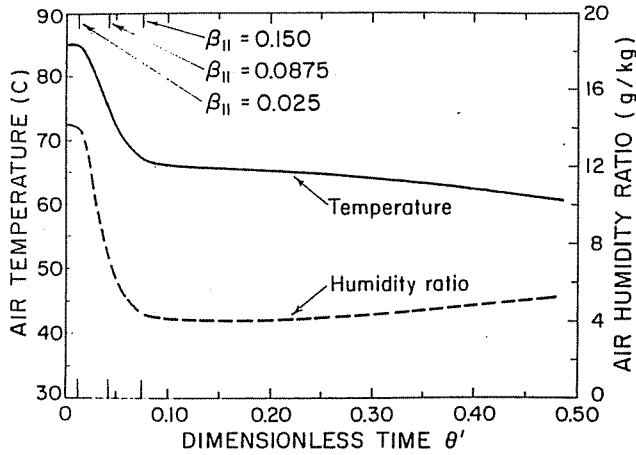


Fig. 6 Period 1 outlet temperature and humidity ratio distributions for the preconditioning purge dehumidifier with inlet state pair 1

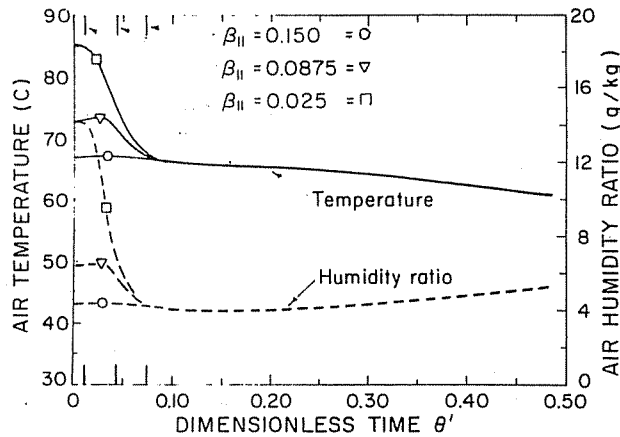


Fig. 7 Period 1 outlet temperature and humidity ratio distributions for the postconditioning purge dehumidifier with inlet state pair 1

period 1 outlet temperature and humidity ratio in this case is much less than 1 percent of the total change in period 1 air state from the inlet conditions. In contrast, the equilibrium solutions for the postconditioning purge showed an effect of  $\beta$  on the period 1 outlet state distributions. The predicted effect is evident in the numerical results given in Fig. 7 and Table 2. For  $\beta = 0.025 < C_{1,1}$ , the postconditioning purge outlet state distributions are essentially identical to those for the preconditioning purge, while for  $\beta = 0.15 > C_{1,1}$  the period 1 outlet temperature and humidity ratio distributions are nearly constant with  $\theta'$  at values near those of the period 1 intersection point. Also in confirmation of the analogy prediction, the data in Table 2 show that a given purge angle there is little difference in the process outlet states for the two geometries. The only feature of the equilibrium solution that is in distinct variance with the finite difference results is the prediction that a minimum in outlet humidity ratio is obtained at  $\beta = C_{1,1}$ . The numerical results show that the minimum process outlet humidity ratio is obtained at a value of  $\beta$  greater than  $C_{1,1}$ . This result is due to the continuous nature of the outlet state distributions. On the whole, however, these comparisons of the analogy solutions with the results of the finite difference model confirm the qualitative utility of the equilibrium analysis using the analogy method.

The numerical results show that the process stream outlet humidity ratio decreases with increasing  $\beta$ , which suggests that there is a purge angle which maximizes the dehumidification of the process air stream. However, performance of purged dehumidifiers can be compared on the basis of either constant total flow through the dehumidifier or

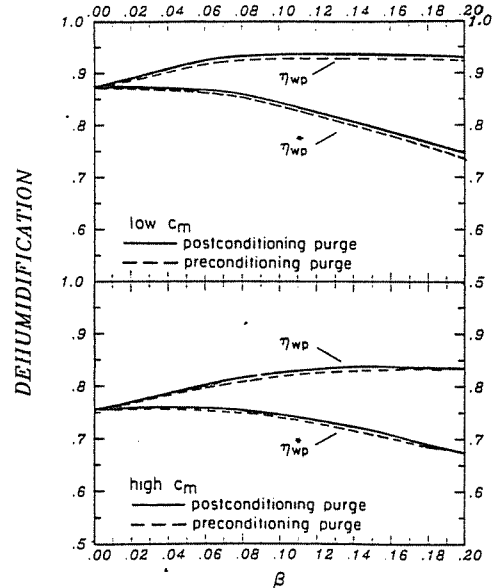


Fig. 8 Normalized dehumidification  $\eta_{wp}$  and  $\eta_{wp}^*$  for low and high thermal capacitance purged dehumidifiers with inlet state pair 1

constant process stream flow rate as the purge fraction is changed.

If the process air flow rate is kept constant as  $\beta$  is increased, then the total flow through the dehumidifier must increase as  $(1-\beta)^{-1}$ . The wheel radius must increase as  $(1-\beta)^{-1/2}$  to keep  $\mu\kappa$  and  $\Lambda$  constant. For constant dehumidifier process stream flow, the dehumidifier efficiency is

$$\eta_{wp} = \frac{w_{1,1} - w_{12,2}}{w_{1,1} - w_{1,int}} \quad (4)$$

where  $w_{1,int}$  is the humidity ratio at the period 1  $F_i$  intersection point. This is a measure of dehumidifier performance provided that the dehumidifier size and the power to pump air through the dehumidifier are unimportant.

If the total air flow through the dehumidifier is kept constant as  $\beta$  is increased, then the dehumidified air flow rate decreases as  $(1-\beta)$ . In this case, the effective humidification per unit total process period flow is

$$\eta_{wp}^* = (1-\beta)\eta_{wp} = (1-\beta) \frac{w_{1,1} - w_{12,2}}{w_{1,1} - w_{1,int}} \quad (5)$$

This figure of merit is appropriate if the dehumidifier is of specified diameter or if the power requirement to pump air through the matrix is important.

The effects of purge angle  $\beta$  and purge geometry on the efficiencies  $\eta_{wp}$  and  $\eta_{wp}^*$  for a purged dehumidifier with inlet state 1 are illustrated in Fig. 8. The data show that the postconditioning recirculation pattern consistently results in a slightly drier process outlet state than does the preconditioning purge. For both the low and high thermal capacitance dehumidifiers, a minimum in process stream humidity ratio is obtained at  $\beta = 0.125$ . This purge angle is greater than the optimum predicted by the equilibrium analogy analysis for either matrix. The maxima in dehumidification per unit process flow rate,  $\eta_{wp}$ , for the low and high thermal capacitance dehumidifiers are respectively 7 percent and 11 percent greater than the  $\eta_{wp}$  obtained with unpurged operation. Although the high thermal capacitance dehumidifier benefits more from purging than does the low thermal capacitance dehumidifier, the low thermal capacitance matrix still results in the greater dehumidification. Also, while there are maxima in  $\eta_{wp}$  for the two matrices, the  $\eta_{wp}^*$  decrease monotonically with increasing  $\beta$ . For inlet state pair 1, at fixed total flow through the matrix,

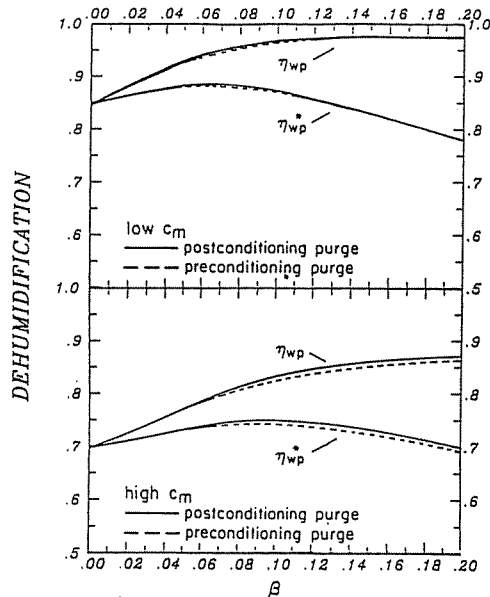


Fig. 9 Normalized dehumidification  $\eta_{wp}$  and  $\eta_{wp}^*$  for low and high thermal capacitance purged dehumidifiers with inlet state pair 2

the process stream flow rate decreases more rapidly with increasing purge angle than does the outlet humidity ratio, resulting in a net decrease in useful dehumidification.

The corresponding results for inlet state pair 2 are illustrated in Fig. 9. The postconditioning recirculation again results in slightly greater dehumidification than does the preconditioning purge. The minima in process stream outlet humidity ratio occur at  $\beta = 0.175$  and  $\beta > 0.20$  for the low and high thermal capacitance matrices, respectively. These angles are greater than those required for inlet state pair 1, and are nearly twice the optimum values predicted by the equilibrium analogy. The corresponding maxima in  $\eta_{wp}$  are 15 and 25 percent greater than obtained with an unpurged dehumidifier. As was the case previously, the high thermal capacitance matrix results in poorer dehumidification than the low thermal capacitance matrix. However, in contrast to the results for inlet state pair 1, there are also maxima in the dehumidification per unit total period 1 flow,  $\eta_{wp}^*$ . These maxima are 4 and 8 percent greater than the  $\beta = 0.0$  values for the two matrices, and occur at values of  $\beta$  less than those corresponding to the maxima in process stream outlet humidity ratio.

The finite difference solution indicates that the recirculated purge improves the dehumidifier performance for inlet state pair 2 more than for inlet state pair 1. This is due to the much greater difference between regenerating inlet and the process inlet humidity ratios for inlet state pair 2. The significance of these improvements in dehumidifier performance depends on the constraints imposed on the dehumidifier design and operating conditions.

For example, suppose that the inlet states are fixed at state pair 2, and the dehumidifier performance can only be modified by changing the flow length,  $\Lambda_{jk}$ . For both the low and high thermal capacitance matrices,  $\Lambda_{jk}$  must be increased to more than 80 in order for an unpurged ( $\beta = 0$ ) dehumidifier to have the same dehumidification per unit period flow as the optimum purged dehumidifier with  $\Lambda_{jk} = 20$ . This represents a substantial change in dehumidifier geometry.

Alternatively, if the dehumidifier dimensions and flow rates are fixed, the regeneration temperature of the unpurged low thermal capacitance dehumidifier must be boosted from 85 to 88.5°C in order to give the same performance as the optimum purged dehumidifier with an 85°C regeneration temperature. Similarly, the regeneration temperature of the unpurged high

thermal capacitance dehumidifier must be increased from 85 to 89.5°C. The unpurged dehumidifier requires a greater input of thermal energy to the regenerating stream to match purged dehumidifier performance, not only because the required regeneration temperatures are higher, but because the regenerating flow rate is greater than in the purged dehumidifier by a factor of  $(1 - \beta)^{-1}$ . For inlet state pair 2, the energy requirement for an unpurged flow capacitance dehumidifier is at least 6 percent greater than that of the optimum purged dehumidifier, while the unpurged high capacitance dehumidifier requires over 10 percent more energy input than the equivalent purged dehumidifier. If the purged dehumidifier is coupled with a regenerative heat exchanger, the proportional energy savings can be greater than those indicated here.

## Summary and Conclusions

The performance of a purged counterflow dehumidifier with recirculation of purged flow to produce a spatially nonuniform inlet condition in the regenerating period inlet was studied using both an equilibrium analysis and a finite difference model of the dehumidifier. This study has quantitatively shown that dehumidifier performance can be improved by purge recirculation.

The wave diagram solutions show that in an equilibrium system, the process stream outlet state is independent of the purge geometry and depends only on the purge angle. The period 1 outlet state distribution is not affected by the preconditioning purge recirculation but is changed by the postconditioning purge flow. A minimum in the process stream outlet humidity ratio occurs at  $\beta = C_{1,1}$ .

The finite difference model of the dehumidifier verified the trends predicted by the equilibrium analysis. The numerical solution shows that the dehumidifier performance is affected by the purge angle but is only slightly influenced by purge geometry. The postconditioning purge geometry consistently results in slightly lower process stream outlet humidity ratios than can be obtained with the preconditioning flow. The period 1 outlet state distribution is insensitive to purge angle  $\beta$  in the preconditioning purge but varies with  $\beta$  in the postconditioning purge recirculation. The minimum in process stream outlet humidity ratio occurs at values of  $\beta$  greater than predicted by the equilibrium analysis.

For silica gel dehumidifier with  $Le_o = 1$  and with either a low or high thermal capacitance matrix, the recirculated purge dehumidifier has lower process stream outlet humidity ratios than the unpurged dehumidifier. However, for a constant total air flow rate, purged operation improves dehumidification capacity only if the regenerating inlet state humidity ratio is considerably greater than the process stream inlet humidity ratio. For the two inlet states considered, the maximum increase in dehumidification per unit period flow rate was 4 percent for the low thermal capacitance dehumidifier and 8 percent for the high thermal capacitance dehumidifier. The purged high thermal capacitance dehumidifier results in poorer dehumidification than can be obtained with the low thermal capacitance matrix.

## Acknowledgments

The authors thank Drs. D. J. Close, P. J. Banks, and J. G. van Leersum of CSIRO Division of Energy Technology, Dr. M. J. Brandemuehl of Carrier Corporation, and Professor W. A. Beckman, University of Wisconsin, for their comments on this work. This project was supported by the Solar Heating and Cooling Research and Development Branch, Office of Conservation and Solar Applications, U.S. Department of Energy.

## References

- 1 Product literature, TB-75, 330, Cargocaire Engineering Corp., Amesbury, Mass.
- 2 Nelson, J. S., Beckman, W. A., Mitchell, J. W., and Close, D. J., "Simulation of the Performance of Open-Cycle Desiccant Systems Using Solar Energy," *Solar Energy*, Vol. 21, 1978, pp. 273-278.
- 3 Jurinak, J. J., Mitchell, J. W., and Beckman, W. A., "Open-Cycle Desiccant Air Conditioning as an Alternative to Vapor Compression Cooling in Residential Application," *Solar Eng. 1983, Proc. ASME Solar Energy Div., 5th Annual Conf.*, Orlando, Fl., Apr. 1983, pp.1-9.
- 4 Macriss, R. A., and Zawacki, T. S., "High COP Rotating Wheel Solid Desiccant System," *Proc. 9th Energy Technology Conf.*, Washington, D.C., Feb. (1982).
- 5 Gunderson, M. E., Huang, K. C., and Railing, S. M., "Development of a Solar Desiccant Dehumidifier, Vol. 1 and 2," SAN-1591-1, Mar. 1978.
- 6 Jurinak, J. J., and Mitchell, J. W., "Effect of Matrix Properties on the Performance of a Counterflow Rotary Dehumidifier," *Heat Transfer in Porous Media*, ASME 1982 Winter Annual Meeting, Vol. HTD-22, Nov. 1982, pp. 69-79; accepted for publication in the ASME JOURNAL OF HEAT TRANSFER.
- 7 Barlow, R. S., and Collier, R. K., "Optimizing the Performance of Desiccant Beds for Solar Regenerated Cooling," *Proceedings of the 1981 Annual Meeting of AS/ISES*, Philadelphia, 1981.
- 8 Mei, V., and Lavan, Z., "Performance of Cross-Cooled Desiccant Dehumidifiers," Paper No. 80-WA/Sol-34, ASME Winter Annual Meeting, Chicago, Nov. 1980.
- 9 Maclaine-cross, I. L., "A Theory of Combined Heat and Mass Transfer in Regenerators," PhD thesis, Department of Mechanical Engineering, Monash University, Clayton, Victoria, Australia, 1974.
- 10 Holmberg, R. B., "Combined Heat and Mass Transfer in Regenerators with Hygroscopic Materials," ASME JOURNAL OF HEAT TRANSFER, Vol. 101, May 1979, pp. 205-210.
- 11 Barlow, R. S., "Analysis of the Adsorption Process and of Desiccant Cooling Systems—Pseudo-Steady-State Model for Coupled Heat and Mass Transfer," SERI/TR-631-1330, Dec. 1981.
- 12 Brandemuehl, M. J., and Banks, P. J., "Rotary Heat Exchangers with Time Varying or Nonuniform Inlet Temperatures," *Regenerative and Recuperative Heat Exchangers*, HTD-21, ASME 1981 Winter Annual Meeting, Nov. 1981.
- 13 Jurinak, J. J., "Open-Cycle Solid Desiccant Cooling—Component Models and System Simulations," PhD thesis, Department of Mechanical Engineering, University of Wisconsin-Madison, 1982.
- 14 Maclaine-cross, I. L., and Banks, P. J., "Coupled Heat and Mass Transfer in Regenerators—Prediction Using an Analogy With Heat Transfer," *Int'l Jour Heat Mass Trans.*, Vol. 15, 1972, pp. 1225-1242.
- 15 Banks, P. J., "Prediction of Heat and Water Vapour Exchanger Performance from That of a Similar Heat Exchanger," *Compact Heat Exchanger—History, Technological Advancement and Mechanical Design Problems*, HTD-10, ASME 1980 Winter Annual Meeting, Nov. 1980, pp. 57-64.
- 16 Banks, P. J., "Coupled Equilibrium Heat and Single Adsorbate Transfer in Fluid Flow through a Porous Medium: 1. Characteristic Potentials and Specific Capacity Ratios," *Chem. Eng. Sci.*, Vol. 27, May 1972, pp. 1143-1150.
- 17 Jurinak, J. J., and Banks, P. J., "An Evaluation of Two Analogy Solutions for a Counterflow Rotary Silica Gel Dehumidifier," *Heat Transfer in Porous Media*, Vol. HTD-22, ASME 1982 Winter Annual Meeting, Nov. 1982, pp. 57-68.
- 18 Close, D. J., CSIRO Div. Energy Technology, Highett, Vic. Australia, personal communication, 1981.
- 19 Brandemuehl, M. J., "Analysis of Heat and Mass Transfer Regenerators with Time Varying or Spatially Nonuniform Inlet Conditions," PhD thesis, Department of Mechanical Engineering, University of Wisconsin-Madison, 1981.

